Inorganic Chemistry
Article

Inorg. Chem. 2011, 50, 1905–1913 1905
DOI: 10.1021/ic102387x

Spin Crossover in Tetranuclear Cyanide-Bridged Iron(II) Square Complexes: A Theoretical Study

Ekaterina M. Zueva,*,† Elmira R. Ryabikh,† Andrey M. Kuznetsov,† and Serguei A. Borshch*,‡

†*Department of Inorganic Chemistry, Kazan State Technological University, 68 K. Marx Street, 420015 Kazan, Russia, and* ‡*Laboratoire de Chimie, UMR 5182, Ecole Normale Supérieure de Lyon, 46 allée d'Italie, 69364 Lyon Cedex 07, France*

Received November 30, 2010

Spin crossover in a series of six cyanide-bridged iron(II) tetranuclear square complexes was analyzed using density functional theory (DFT) methods. As the spin crossover between the low-spin (LS) and high-spin (HS) states can occur only for two of four iron ions, we characterized energetically and structurally the [LS−LS], [HS−LS], and [HS−HS] spin-state isomers. For all studied complexes, the energy of the mixed [HS−LS] spin state does not deviate essentially from the halfway point between the energies of homogeneous spin states, thereby satisfying the conditions for an one-step transition between the [LS−LS] and [HS−HS]. This fact reflects the weak elastic coupling between the environments of transiting centers. The two-step spin transition observed in one complex can appear only due to the crystal packing effects. We also evaluated the strength of exchange coupling between the paramagnetic ions in the [HS−HS] state.

Introduction

The phenomenon of thermal spin transition between low-spin (LS) and high-spin (HS) electronic states discovered in iron(III) dithiocarbamate complexes in 1931[1] has been extensively studied during the past two decades.[2−11] Many other mononuclear spin-crossover (SCO) compounds, mainly iron(II) and iron(III), to a lesser extent cobalt(II), and only a few manganese(II), manganese(III), chromium(II), and cobalt(III) complexes, have been reported. These studies provided a deeper insight into the microscopic mechanism of this phenomenon. Basically, the spin transition is a property of the isolated complex.[12] However, the network of intermolecular contacts in the crystal lattice is responsible for the cooperativity defined as a communication medium among the metal active sites during the SCO process (the stronger the intermolecular interactions, the more cooperative the spin transition). To be used in molecular electronics, the thermal spin transition must be abrupt with well-defined hysteresis loop. Numerous attempts have been made to build highly cooperative SCO systems. It was found that, due to a noncovalent nature of intermolecular interactions, their spreading in the crystal lattice is difficult to control.[13] To enhance cooperativity relative to mononuclear SCO compounds, it was suggested to link the metal active sites by covalent bridges.[14] The experimental work in this direction has resulted in a number of polymeric[6,11,15−19] and polynuclear (mainly, binuclear)[7,9,11,20−28] systems.

One of the most interesting features of binuclear SCO systems is the manifestation of three spin-pair states, namely

*Corresponding authors. E-mail: borchtch@ens-lyon.fr (S.A.B.); zueva_ekaterina@mail.ru (E.M.Z.).

(1) (a) Cambi, L.; Szegö, L.; Cagnasso, A. *Atti Accad. Naz. Lincei* **1931**, *13*, 168. (b) Cambi, L.; Szegö, L. *Atti Accad. Naz. Lincei* **1932**, *15*, 329. (c) Cambi, L.; Szegö, L. *Atti Accad. Naz. Lincei* **1932**, *15*, 599.
(2) Spin Crossover in Transition Metal Compounds. In *Topics in Current Chemistry*; Gütlich, P., Goodwin, H. A., Eds.; Springer-Verlag: Berlin, Heidelberg, 2004; pp 233−235.
(3) Bousseksou, A.; Molnár, G.; Matouzenko, G. S. *Eur. J. Inorg. Chem.* **2004**, 4353.
(4) Gütlich, P.; Koningsbruggen, P. J. v.; Renz, F. *Struct. Bonding* (*Berlin*) **2004**, *107*, 27.
(5) Gaspar, A. B.; Ksenofontov, V.; Seredynyuk, M.; Gütlich, P. *Coord. Chem. Rev.* **2005**, *249*, 2661.
(6) Real, J. A.; Gaspar, A. B.; Muñoz, M. C. *Dalton Trans.* **2005**, 2062.
(7) Gaspar, A. B.; Muñoz, M. C.; Real, J. A. *J. Mater. Chem.* **2006**, *16*, 2522.
(8) Sorai, M.; Nakano, M.; Miyazaki, Y. *Chem. Rev.* **2006**, *106*, 976.
(9) Bousseksou, A.; Molnár, G.; Real, J. A.; Tanaka, K. *Coord. Chem. Rev.* **2007**, *251*, 1822.
(10) Halcrow, M. A. *Polyhedron* **2007**, *26*, 3523.
(11) Murray, K. S. *Eur. J. Inorg. Chem.* **2008**, 3101.
(12) Hauser, A. *Top. Curr. Chem.* **2004**, *233*, 49.
(13) (a) Matouzenko, G. S.; Bousseksou, A.; Lecocq, S.; Koningsbruggen, P. J. v.; Perrin, M.; Kahn, O.; Collet, A. *Inorg. Chem.* **1997**, *36*, 5869. (b) Matouzenko, G. S.; Létard, J.-F.; Bousseksou, A.; Lecocq, S.; Capes, L.; Salmon, L.; Perrin, M.; Kahn, O.; Collet, A. *Eur. J. Inorg. Chem.* **2001**, *11*, 2935.
(14) (a) Kahn, O.; Codjovi, E. *Philos. Trans. R. Soc. London A* **1996**, *354*, 359. (b) Kahn, O.; Garcia, Y.; Létard, J.-F.; Mathonière, C. *NATO ASI Ser. C* **1998**, *518*, 127.
(15) García, Y.; Niel, V.; Muñoz, M. C.; Real, J. A. *Top. Curr. Chem.* **2004**, *233*, 229.
(16) Real, J. A.; Gaspar, A. B.; Niel, V.; Muñoz, M. C. *Coord. Chem. Rev.* **2003**, *235*, 121.
(17) (a) Matouzenko, G. S.; Molnár, G.; Bréfuel, N.; Perrin, M.; Bousseksou, A.; Borshch, S. A. *Chem. Mater.* **2003**, *15*, 550. (b) Matouzenko, G. S.; Perrin, M.; Le Guennic, B.; Genre, C.; Molnár, G.; Bousseksou, A.; Borshch, S. A. *Dalton Trans.* **2007**, 934.

Published on Web 01/27/2011

[HS−HS], [HS−LS], and [LS−LS]. The important consequence of the presence of three spin-pair states is the existence of different types of SCO. One of them is a usual one-step SCO [HS−HS] → [LS−LS]. Two other types of spin transition directly involve the mixed [HS−LS] state. The transition can occur in two steps, [HS−HS] → [HS−LS] → [LS−LS], when the mixed state is stabilized on the intermediate plateau of the magnetic curve. In this case, the SCO molecule can be seen not as a bistable but as a multistable system. Finally, a half SCO [HS−HS] → [HS−LS] can take place. It is important to note that the mixed spin state can be stabilized even in cases when in the [HS−HS] and [LS−LS] states both centers are strictly identical. The thermodynamical model developed in ref 20 demonstrated that the [HS−LS] state enthalpy must be lower than the halfway point between the enthalpies of [LS−LS] and [HS−HS] states to have a two-step spin transition. The DFT calculations for a series of binuclear complexes demonstrated the validity of this energetic criterion for two-step SCO.[29] In a recent paper,[28] the analysis of available structural data for numerous binuclear complexes allowed to conclude that the nature of SCO in binuclear compounds is determined by intramolecular factors. The stabilization of the intermediate [HS−LS] state is due to the distortion of the geometry around the HS center induced by the SCO on the neighbor and conditioned by the strain effects in bridging and terminal ligands. Thus, the nature of SCO depends on the ligand field strength provided by polydentate ligands more or less strained and also on the ability of ligands to perform distortions necessary for the spin state transformation.

Scheme 1

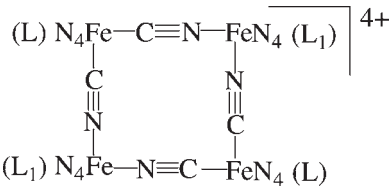

Recently, a new type of polynuclear iron(II) SCO complex emerged, namely [2 × 2] grids or tetranuclear square complexes.[30−38] Four iron(II) centers are bridged either by extended organic ligands[30−33] or by cyanide ions,[34−38] and their coordination spheres are completed by polydentate nitrogen-containing ligands. In the case of CN bridges (Scheme 1), the carbon atoms produce a stronger ligand field, and the iron centers coordinated by these atoms remain in the LS state if a cyanide flip found in several solid and molecular analogues of Prussian blue[39,40] does not occur. The SCO can take place only on two iron(II) centers, and these compounds can be considered as a particular case of binuclear SCO systems. To our knowledge, six examples of CN-bridged iron(II) squares have been reported in the literature. In the $[Fe_4(\mu\text{-}CN)_4(bpy)_8](PF_6)_4\cdot 4H_2O$ complex (**1**$(PF_6)_4\cdot 4H_2O$, bpy = 2,2′-bipyridine), both SCO centers remain in the LS state in the whole temperature range studied (2−300 K).[34] The tetranuclear species in the $[Fe_4(\mu\text{-}CN)_4(bpy)_4(bpym)_4](PF_6)_4\cdot 6CH_3OH\cdot 4H_2O$ complex (**2**$(PF_6)_4\cdot 6CH_3OH\cdot 4H_2O$) contains the 2,2′-bipyrimidine (bpym) ligands at the transiting centers and undergoes a reversible one-step SCO [LS−LS] ↔ [HS−HS]; however, the characteristic temperature is very high (this complex is diamagnetic below 250 K; $\chi_{mol}T$ is equal to 1.0 cm^3 K mol^{-1} at 300 K).[38] The $[Fe_4(\mu\text{-}CN)_4(bpy)_4(tpma)_2]^{4+}$ complex (**3**) obtained as the BF_4^- and PF_6^- salts[35,36] contains the tris(pyridin-2-ylmethyl)amine (tpma) ligands at the transiting centers. Magnetic susceptibility measurements carried out for the PF_6^- salt[36] clearly show the occurrence of a reversible two-step SCO [LS−LS] ↔ [HS−LS] ↔ [HS−HS] ($T_{1/2}(1)$ = 160 K, $T_{1/2}(2) \approx$ 380 K) in this compound; the plateau corresponding to the [HS−LS] phase has a width of ∼100 K. The 1,10-phenanthroline (phen) derivative of **3**, where the bpy ligands at the non-SCO centers are replaced by the phen ligands, $[Fe_4(\mu\text{-}CN)_4(phen)_4(tpma)_2]^{4+}$ (**4**), was obtained as the PF_6^- salt by Real and co-workers.[37] The spin conversion of **4**$(PF_6)_4$ occurs in one step [LS−LS] ↔ [HS−HS] at the characteristic temperature close to that of the high-temperature step in **3**$(PF_6)_4$. The last

(18) (a) Genre, C.; Matouzenko, G. S.; Jeanneau, E.; Luneau, D. *New J. Chem.* **2006**, *30*, 1669. (b) Genre, C.; Jeanneau, E.; Bousseksou, A.; Luneau, D.; Borshch, S. A.; Matouzenko, G. S. *Chem.—Eur. J.* **2008**, *14*, 697.
(19) Neville, S. M.; Leita, B. A.; Halder, G. J.; Kepert, C. J.; Moubaraki, B.; Létard, J.-F.; Murray, K. S. *Chem.—Eur. J.* **2008**, *14*, 10123.
(20) Real, J. A.; Bolvin, H.; Bousseksou, A.; Dworkin, A.; Kahn, O.; Varret, F.; Zarembowitch, J. *J. Am. Chem. Soc.* **1992**, *114*, 4650.
(21) Real, J. A.; Gaspar, A. B.; Muñoz, M. C.; Gütlich, P.; Ksenofontov, V.; Spiering, H. *Top. Curr. Chem.* **2004**, *233*, 167.
(22) Murray, K. S.; Kepert, C. J. *Top. Curr. Chem.* **2004**, *233*, 195.
(23) (a) Suemura, N.; Ohama, M.; Kaizaki, S. *Chem. Commun.* **2001**, 1538. (b) Nakano, K.; Suemura, N.; Kawata, S.; Fuyuhiro, A.; Yagi, T.; Nasu, S.; Morimoto, S.; Kaizaki, S. *Dalton Trans.* **2004**, 982. (c) Nakano, K.; Kawata, S.; Yoneda, K.; Fuyuhiro, A.; Yagi, T.; Nasu, S.; Morimoto, S.; Kaizaki, S. *Chem. Commun.* **2004**, 2892. (d) Nakano, K.; Suemura, N.; Yoneda, K.; Kawata, S.; Kaizaki, S. *Dalton Trans.* **2005**, 740. (e) Yoneda, K.; Adachi, K.; Hayami, S.; Maeda, Y.; Katada, M.; Fuyuhiro, A.; Kawata, S.; Kaizaki, S. *Chem. Commun.* **2006**, 45.
(24) Létard, J.-F.; Carbonera, C.; Real, J. A.; Kawata, S.; Kaizaki, S. *Chem.—Eur. J.* **2009**, *15*, 4146.
(25) Schneider, C. J.; Cashion, J. D.; Moubaraki, B.; Neville, S. M.; Batten, S. R.; Turner, D. R.; Murray, K. S. *Polyhedron* **2007**, *26*, 1764.
(26) Fedaoui, D.; Bouhadja, Y.; Kaiba, A.; Guionneau, P.; Létard, J.-F.; Rosa, P. *Eur. J. Inorg. Chem.* **2008**, 1022.
(27) Ortega-Villar, N.; Thompson, A. L.; Muñoz, M. C.; Ugalde-Saldívar, V. M.; Goeta, A. E.; Morena-Esparza, R.; Real, J. A. *Chem.—Eur. J.* **2005**, *11*, 5721.
(28) Verat, A. Yu.; Ould-Moussa, N.; Jeanneau, E.; Le Guennic, B.; Bousseksou, A.; Borshch, S. A.; Matouzenko, G. S. *Chem.—Eur. J.* **2009**, *15*, 10070.
(29) Zein, S.; Borshch, S. A. *J. Am. Chem. Soc.* **2005**, *127*, 16197.
(30) (a) Breuning, E.; Ruben, M.; Lehn, J. M.; Renz, F.; Garcia, Y.; Ksenofontov, V.; Gütlich, P.; Wegelius, E.; Rissanen, K. *Angew. Chem., Int. Ed.* **2000**, *39*, 2504. (b) Ruben, M.; Breuning, E.; Lehn, J. M.; Ksenofontov, V.; Renz, F.; Gütlich, P.; Vaughan, G. B. M. *Chem.—Eur. J.* **2003**, *9*, 4422. (c) Alam, M. S.; Strömsdörfer, S.; Dremov, V.; Müller, P.; Kortus, J.; Ruben, M.; Lehn, J. M. *Angew. Chem., Int. Ed.* **2005**, *44*, 7896. (d) Ruben, M.; Ziener, U.; Lehn, J. M.; Ksenofontov, V.; Gütlich, P.; Vaughan, G. B. M. *Chem.—Eur. J.* **2005**, *11*, 94.
(31) Wu, D.-Y.; Sato, O.; Einaga, Y.; Duan, C.-Y. *Angew. Chem., Int. Ed.* **2009**, *48*, 1475.
(32) Shuvaev, K. V.; Dawe, L. N.; Thompson, L. K. *Dalton Trans.* **2010**, 4768.
(33) Schneider, B.; Demeshko, S.; Dechert, S.; Meyer, F. *Angew. Chem., Int. Ed.* **2010**, *49*, 9274–9277.
(34) Oshio, H.; Onodera, H.; Tamada, O.; Mizutani, H.; Hikichi, T.; Ito, T. *Chem.—Eur. J.* **2000**, *6*, 2523.
(35) Flay, M.-L.; Comte, V.; Vahrenkamp, H. *Z. Anorg. Allg. Chem.* **2003**, *629*, 1147.
(36) Nihei, M.; Ui, M.; Yokota, M.; Han, L.; Maeda, A.; Kishida, H.; Okamoto, H.; Oshio, H. *Angew. Chem., Int. Ed.* **2005**, *44*, 6484.
(37) Boldog, I.; Muñoz-Lara, F. J.; Gaspar, A. B.; Muñoz, M. C.; Seredyuk, M.; Real, J. A. *Inorg. Chem.* **2009**, *48*, 3710.
(38) Nihei, M.; Ui, M.; Oshio, H. *Polyhedron* **2009**, *28*, 1718.
(39) Coronado, E.; Gimenez-Lopez, M. C.; Levchenko, G.; Romero, F. M.; Garcia-Baonza, V.; Milner, A.; Paz-Pasternak, M. *J. Am. Chem. Soc.* **2005**, *127*, 4580.
(40) Shatruk, M.; Dragulescu-Andrasi, A.; Chambers, K. E.; Stoian, S. A.; Bominaar, E. L.; Achim, C.; Dunbar, K. R. *J. Am. Chem. Soc.* **2007**, *129*, 6104.

two examples (**5** and **6**) obtained as the $[Fe_4(\mu\text{-}CN)_4(phen)_4(Me\text{-}tpma)_2](PF_6)_4$ and $[Fe_4(\mu\text{-}CN)_4(phen)_4(Me_2\text{-}tpma)_2](PF_6)_4 \cdot NH_4PF_6$ compounds are similar to **4** but contain Me-substituted tpma ligands (Me-tpma = 6-methylpyrid-2-ylmethyl)bis(pyrid-2-ylmethyl)amine, Me_2-tpma = bis(6-methylpyrid-2-ylmethyl)(pyrid-2-ylmethyl)amine).[37] These complexes are in the [HS−HS] state in the whole temperature range studied (4−400 K).

The previous studies[28,29] have shown that quantum-chemical calculations provide a useful tool to describe the energetics of binuclear SCO species and to provide a structural information for all spin states, which is not always available from X-ray crystallography. In the present paper, we perform the quantum-chemical analysis to characterize structurally (through the geometry optimization) and energetically possible spin states for a series of CN-bridged iron(II) square complexes (**1**−**6**). The goal of such analysis is to elucidate the role of the topology and the particular bridging pathway between the transiting centers in the SCO behavior. As the calculations concern molecules in the gas phase, they allow to separate effects inherent to isolated molecules and those resulting from the crystal environment. We also evaluate the strength of exchange interactions between iron(II) ions active in the [HS−HS] state.

Theoretical Details

Calculations reported in this paper were performed within the DFT framework using the PRIRODA[41,42] (version 5.0[43]) and GAUSSIAN03[44] packages. The choice of the better-suited exchange-correlation functional for the description of SCO complexes has been widely debated in the literature,[45] but the complete consensus has not yet been achieved. In the present study, we used different functionals (OLYP,[46,47] OPBE,[46,48,49] PBE,[48,49] B3LYP*[50]) proved to be the best-performing for a number of previously studied SCO complexes[45] and examined their performance for the given CN-bridged iron(II) square complexes. Different all-electron GTO basis sets were used, namely the so-called 3z[51] (of TZ2P quality) and L2[52] (compatible with cc-pVTZ) basis sets implemented in the PRIRODA package, whereas the GAUSSIAN03 calculations were carried out using the TZVP basis set reported by Ahlrichs and co-workers.[53]

Geometry Optimizations. Full geometry optimizations were mostly performed using the highly effective PRIRODA code, which employs the expansion of the electron density in an auxiliary basis set to accelerate evaluation of the Coulomb and exchange-correlation terms.[41] The B3LYP* calculations were done using the GAUSSIAN03 program. An extended series of test calculations (PBE/3z, PBE/L2, OLYP/3z, OLYP/L2, B3LYP*/TZVP) were carried out for the $[Fe_4(\mu\text{-}CN)_4(bpy)_4(tpma)_2]^{4+}$ complex. The key structural parameters optimized for the [LS−LS] and [HS−LS] states, along with the X-ray crystallographic data, are given in Tables S1 and S2 of the Supporting Information. From these tables it can be seen that the experimental structures are best reproduced within the PBE framework. The influence of the basis set size (3z versus L2) is negligible. A series of geometry optimizations (OLYP/3z, PBE/3z) were also carried out for the $[Fe_4(\mu\text{-}CN)_4(bpy)_8]^{4+}$ complex. As for the previous case, the PBE functional provides better performance. Therefore, the geometries of all other representatives of the series (for all spin states) were optimized within the framework of the PBE/3z computational procedure.

Single Point Energy Calculations. A series of test SCF calculations (PBE/TZVP, PBE/L2, OLYP/TZVP, OLYP/L2, OPBE/TZVP, B3LYP*/TZVP) were carried out for the $[Fe_4(\mu\text{-}CN)_4(bpy)_4(tpma)_2]^{4+}$ complex. The energy gaps between different spin states calculated for optimized and experimental structures are given in Table S3 of the Supporting Information. Each method gives similar results for all optimized geometries. The PBE functional favors the $S = 0$ local state leading to the ΔE values, which are too large (the energy gaps are especially large for the crystal structures), whereas the OLYP, OPBE, and B3LYP* functionals give much smaller ΔE values for the crystal structures and even inversion of spin levels for the isolated complexes (i.e., $E_{HH} < E_{HL} < E_{LL}$), contrary to what is observed experimentally. The structural distortion of the complex induced by the crystal lattice is not so pronounced to cause the inversion of spin levels. Therefore, these methods seem to stabilize the $S = 2$ local state. An additional series of test SCF calculations carried out for the $[Fe_4(\mu\text{-}CN)_4(bpy)_8]^{4+}$ and $[Fe_4(\mu\text{-}CN)_4(phen)_4(tpma)_2]^{4+}$ complexes confirm the above conclusions about the performance of different DFT functionals. Although the

(41) Laikov, D. N. *Chem. Phys. Lett*. **1997**, *281*, 151.
(42) Laikov, D. N.; Ustynyuk, Y. A. *Russ. Chem. Bull., Int. Ed.* **2005**, *54*, 820.
(43) Laikov, D. N. PRIRODA, Electronic Structure Code, Version 5, 2005.
(44) Frisch, M. J.; Trucks, G. W.; Schlegel, H. B.; Scuseria, G. E.; Robb, M. A.; Cheeseman, J. R.; Montgomery Jr., J. A.; Vreven, T.; Kudin, K. N.; Burant, J. C.; Millam, J. M.; Iyengar, S. S.; Tomasi, J.; Barone, V.; Mennucci, B.; Cossi, M.; Scalmani, G.; Rega, N.; Petersson, G. A.; Nakatsuji, H.; Hada, M.; Ehara, M.; Toyota, K.; Fukuda, R.; Hasegawa, J.; Ishida, M.; Nakajima, T.; Honda, Y.; Kitao, O.; Nakai, H.; Klene, M.; Li, X.; Knox, J. E.; Hratchian, H. P.; Cross, J. B.; Bakken, V.; Adamo, C.; Jaramillo, J.; Gomperts, R.; Stratmann, R. E.; Yazyev, O.; Austin, A. J.; Cammi, R.; Pomelli, C.; Ochterski, J. W.; Ayala, P. Y.; Morokuma, K.; Voth, G. A.; Salvador, P.; Dannenberg, J. J.; Zakrzewski, V. G.; Dapprich, S.; Daniels, A. D.; Strain, M. C.; Farkas, O.; Malick, D. K.; Rabuck, A. D.; Raghavachari, K.; Foresman, J. B.; Ortiz, J. V.; Cui, Q.; Baboul, A. G.; Clifford, S.; Cioslowski, J.; Stefanov, B. B.; Liu, G.; Liashenko, A.; Piskorz, P.; Komaromi, I.; Martin, R. L.; Fox, D. J.; Keith, T.; Al-Laham, M. A.; Peng, C. Y.; Nanayakkara, A.; Challacombe, M.; Gill, P. M. W.; Johnson, B.; Chen, W.; Wong, M. W.; Gonzalez, C.; Pople, J. A. *GAUSSIAN 03, Revision D.01*; Gaussian, Inc.: Wallingford, CT, 2004.
(45) (a) Reiher, M. *Inorg. Chem*. **2002**, *41*, 6928. (b) Paulsen, H.; Trautwein, A. X. *Top. Curr. Chem*. **2004**, *235*, 197. (c) Fouqueau, A.; Mer, S.; Casida, M. E.; Daku, L. M. L.; Hauser, A.; Mineva, T.; Neese, F. *J. Chem. Phys*. **2004**, *120*, 9473. (d) Fouqueau, A.; Casida, M. E.; Daku, L. M. L.; Hauser, A.; Neese, F. *J. Chem. Phys*. **2005**, *122*, 044110. (e) Daku, L. M. L.; Vargas, A.; Hauser, A.; Fouqueau, A.; Casida, M. E. *ChemPhysChem* **2005**, *6*, 1393. (f) Ganzenmüller, G.; Berkaïne, N.; Fouqueau, A.; Casida, M. E.; Reiher, M. J. *Chem. Phys*. **2005**, *122*, 234321. (g) Pierloot, K.; Vancoillie, S. *J. Chem. Phys*. **2006**, *125*, 124303. (h) Zein, S.; Borshch, S. A.; Fleurat-Lessard, P.; Casida, M. E.; Chermette, H. *J. Chem. Phys*. **2007**, *126*, 014105. (i) Pierloot, K.; Vancoillie, S. *J. Chem. Phys*. **2008**, *128*, 034104. (j) Swart, M. *J. Chem. Theory Comput*. **2008**, *4*, 2057. (k) Güell, M.; Luis, J. M.; Solà, M.; Swart, M. *J. Phys. Chem. A* **2008**, *112*, 6384. (l) Jensen, K. P.; Cirera, J. *J. Phys. Chem. A* **2009**, *113*, 10033. (m) Ye, S.; Neese, F. *Inorg. Chem*. **2010**, *49*, 772.
(46) Handy, N. C.; Cohen, A. J. *Mol. Phys*. **2001**, *99*, 403.
(47) Lee, C.; Yang, W.; Parr, R. G. *Phys. Rev. B* **1988**, *37*, 785.
(48) Perdew, J. P.; Burke, K.; Ernzerhof, M. *Phys. Rev. Lett*. **1996**, *77*, 3865.
(49) Perdew, J. P.; Burke, K.; Ernzerhof, M. *Phys. Rev. Lett*. **1997**, *78*, 1396.
(50) Reiher, M.; Salomon, O.; Hess, B. A. *Theor. Chem. Acc*. **2001**, *107*, 48.
(51) Laikov, D. N. PhD Thesis, Moscow State University, 2000.
(52) Laikov, D. N. *Chem. Phys. Lett*. **2005**, *416*, 116.
(53) Schafer, A.; Horn, H.; Ahlrichs, R. *J. Chem. Phys*. **1994**, *100*, 5829.

PBE method overestimates the energy gaps $\Delta E_1 = E_{HL} - E_{LL}$ and $\Delta E_2 = E_{HH} - E_{HL}$, the resulting ΔE_1 and ΔE_2 values are expected to incorporate approximately the same amount of error and therefore allow to draw important conclusions based on the relative energies of the [LS−LS], [HS−LS], and [HS−HS] states. We adopt the PBE/L2 computational procedure for single point energy calculations throughout the paper. In all cases, the spin densities at iron centers were found to be about 0 and 3.7 for local spins equal to 0 and 2, respectively.

Exchange Coupling. The strength of exchange interactions effective in the [HS−HS] state was evaluated for optimized (PBE/3z) and available crystal structures using the BS methodology. The schemes proposed by Noodleman and co-workers[54] (eq 1), Ruiz and co-workers[55] (eq 2), and Yamaguchi and co-workers[56] (eq 3) were used:

$$J^{(a)} = \frac{E_{BS} - E_{HS}}{8} \quad (1)$$

$$J^{(b)} = \frac{E_{BS} - E_{HS}}{10} \quad (2)$$

$$J^{(c)} = \frac{2(E_{BS} - E_{HS})}{\langle \boldsymbol{S}^2 \rangle_{HS} - \langle \boldsymbol{S}^2 \rangle_{BS}} \quad (3)$$

The energies of the five spin multiplets resulting from the exchange coupling between the two $S_i = 2$ centers are given by (the total spin value varies from 0 to 4)

$$E(S) = -\frac{J}{2}[S(S+1) - S_1(S_1+1) - S_2(S_2+1)]$$

The above equations were obtained in terms of the Heisenberg−Dirac−van Vleck spin Hamiltonian $\boldsymbol{H} = -J(\mathbf{S}_1 \cdot \mathbf{S}_2)$. All single determinants (HS and BS) were computed within the framework of the UB3LYP/TZVP computational procedure whose reliability has been repeatedly established.[55,57] The computed $\langle \boldsymbol{S}^2 \rangle_{HS}$ and $\langle \boldsymbol{S}^2 \rangle_{BS}$ values (~20.03 and ~4.03) are close to the corresponding expectation values (20 and 4).

Continuous Shape Measures of the FeN_6 Coordination Spheres. The concept of continuous shape measures (CShM) was introduced to characterize the deviation of the coordination polyhedron of a given mononuclear complex from highly symmetrical polyhedra described by a point group.[58] Mathematically, the CShM of the coordination polyhedron Q with the geometric center $\vec{q}_0$ relative to an ideal polyhedron P is expressed as

$$S_Q(P) = \min \left[\frac{\sum_{i=1}^{N} |\vec{q}_i - \vec{p}_i|^2}{\sum_{i=1}^{N} |\vec{q}_i - \vec{q}_0|^2} \right] \times 100$$

where $\vec{q}_i$ and $\vec{p}_i$ are the position vectors for atoms of two polyhedra. Two highly symmetrical polyhedra are specially important for iron SCO complexes with N_6 donor set, namely the ideal octahedron (the point group O_h) and the trigonal prism (the point group D_{3h}). Based on the Tanabe−Sugano diagrams, the dilatation of octahedral coordination sphere is usually associated with the LS → HS transition. It is evident that the coordination core shape does not change along such distortion. However, the HS state can be also stabilized by the trigonal twist, getting away from an octahedron to a trigonal prism. In the case of octahedral complexes formed by three bidentate ligands, this pathway is realized through the well-known Bailar twist. In real compounds, both types of distortion participate in the spin transformation with individual contributions depending on the flexibility of polydentate ligands. The twist distortion pathway can be represented by the curve in the space of octahedral and trigonal prismatic shape measures. It was demonstrated for a series of mononuclear spin transiting complexes that their structures in different spin states are aligned along this curve, approaching the trigonal prism and getting away from the ideal octahedron for the HS state.[59] This behavior is in agreement with a common observation of more symmetrical structures for LS FeN_6 coordination cores.

We apply the CShM method to characterize the shape of coordination polyhedra of transiting centers in the experimental structures of the $[Fe_4(\mu\text{-}CN)_4(bpy)_4(tpma)_2]^{4+}$ complex obtained at 100, 200, and 300 K as well as in the optimized structures for three spin states. The $S(O_h)$ and $S(D_{3h})$ values called in ref 59 octahedricity and prismacity were calculated using the SHAPE program.[60]

Results and Discussion

Selected distances for the PBE/3z-optimized [LS−LS], [HS−LS], and [HS−HS] structures of complexes **1**−**6** are

(54) (a) Noodleman, L.; Norman, J. G., Jr. *J. Chem. Phys.* **1979**, *70*, 4903. (b) Noodleman, L. *J. Chem. Phys.* **1981**, *74*, 5737. (c) Noodleman, L.; Davidson, E. R. *Chem. Phys.* **1986**, *109*, 131. (d) Noodleman, L.; Case, D. A. *Adv. Inorg. Chem.* **1992**, *38*, 423.

(55) (a) Ruiz, E.; Cano, J.; Alvarez, S.; Alemany, P. *J. Comput. Chem.* **1999**, *20*, 1391. (b) Ruiz, E.; Rodriguez-Fortea, A.; Cano, J.; Alvarez, S.; Alemany, P. *J. Comput. Chem.* **2003**, *24*, 982. (c) Ruiz, E.; Alvarez, S.; Cano, J.; Polo, V. *J. Chem. Phys.* **2005**, *123*, 164110.

(56) (a) Soda, T.; Kitagawa, Y.; Onishi, T.; Takano, Y.; Shigeta, Y.; Nagao, H.; Yoshioka, Y.; Yamaguchi, K. *Chem. Phys. Lett.* **2000**, *319*, 223. (b) Shoji, M.; Koizumi, K.; Kitagawa, Y.; Kawakami, T.; Yamanaka, S.; Okumura, M.; Yamaguchi, K. *Chem. Phys. Lett.* **2006**, *432*, 343.

(57) (a) Ruiz, E.; Alemany, P.; Alvarez, S.; Cano, J. *J. Am. Chem. Soc.* **1997**, *119*, 1297. (b) Ruiz, E.; Alemany, P.; Alvarez, S.; Cano, J. *Inorg. Chem.* **1997**, *36*, 3683. (c) Ruiz, E.; Cano, J.; Alvarez, S.; Alemany, P. *J. Am. Chem. Soc.* **1998**, *120*, 11122. (d) Ruiz, E.; Rodriguez-Fortea, A.; Alemany, P.; Alvarez, S. *Polyhedron* **2001**, *20*, 1323. (e) Ruiz, E.; Graaf, C.; Alemany, P.; Alvarez, S. *J. Phys. Chem. A* **2002**, *106*, 4938. (f) Ruiz, E.; Cano, J.; Alvarez, S.; Caneschi, A.; Gatteschi, D. *J. Am. Chem. Soc.* **2003**, *125*, 6791. (g) Ghosh, P.; Bill, E.; Weyhermuller, T.; Neese, F.; Wieghardt, K. *J. Am. Chem. Soc.* **2003**, *125*, 1293. (h) Rodriguez-Fortea, A.; Alemany, P.; Alvarez, S.; Ruiz, E. *Eur. J. Inorg. Chem.* **2004**, 143. (i) Cano, J.; Costa, R.; Alvarez, S.; Ruiz, E. *J. Chem. Theory Comput.* **2007**, *3*, 782. (j) Zueva, E. M.; Borshch, S. A.; Petrova, M. M.; Chermette, H.; Kuznetsov, An. M. *Eur. J. Inorg. Chem.* **2007**, *27*, 4317. (k) Aronica, C.; Chastanet, G.; Zueva, E. M.; Borshch, S. A.; Clemente-Juan, J. M.; Luneau, D. *J. Am. Chem. Soc.* **2008**, *130*, 2365. (l) Zueva, E. M.; Petrova, M. M.; Herchel, R.; Trávníček, Z.; Raptis, R.; Mathivathanan, L.; McGrady, J. E. *Dalton Trans.* **2009**, *30*, 5924.

(58) (a) Avnir, D.; Katzenelson, O.; Keinan, S.; Pinsky, M.; Pinto, Y.; Salomon, Y.; Zabrodsky Hel-Or, H. In *Concepts in Chemistry: A Contemporary Challenge*; Rouvray, D. H., Ed.; Research Studies Press Ltd.: Taunton, England, 1997; Chapter 9, pp 283−324. (b) Zabrodsky, H.; Peleg, S.; Avnir, D. *J. Am. Chem. Soc.* **1992**, *114*, 7843. (c) Alvarez, S.; Avnir, D.; Llunell, M.; Pinsky, M. *New J. Chem.* **2002**, *26*, 996. (d) Alvarez, S.; Alemany, P.; Casanova, D.; Cirera, J.; Llunell, M.; Avnir, D. *Coord. Chem. Rev.* **2005**, *249*, 1693.

(59) Alvarez, S. *J. Am. Chem. Soc.* **2003**, *125*, 6795.

(60) Llunell, M.; Casanova, D.; Cirera, J.; Bofill, M.; Alemany, P.; Alvarez, S.; Pinsky, M.; Avnir, D. SHAPE program, Version 1.1b, Barcelona, 2003.

Table 1. Selected Bond Lengths (Å) in Optimized (PBE/3z) and Experimental Structures of **1**−**6** in the [LS−LS] State[a]

	1	2	3	4	5	6
Fe(1)−N(5)	2.02 (1.98)[b]	2.02 (1.99)[c]	2.02 (1.99)[d]	2.03 (2.00)[e]	2.03	2.03
Fe(1)−N(6)	1.97 (1.97)	1.97 (1.96)	1.97 (1.96)	1.97 (1.96)	1.97	1.98
Fe(1)−N(7)	2.02 (1.96)	2.02 (1.98)	2.02 (1.99)	2.03 (2.00)	2.03	2.03
Fe(1)−N(8)	1.97 (1.95)	1.97 (1.96)	1.96 (1.97)	1.97 (1.92)	1.97	1.97
Fe(1)−C(9)	1.89 (1.90)	1.89 (1.89)	1.90 (1.91)	1.89 (1.92)	1.90	1.90
Fe(1)−C(10)	1.89 (1.91)	1.89 (1.88)	1.90 (1.92)	1.89 (1.89)	1.89	1.89
Fe(2)−N(11)	1.98 (1.98)	1.97 (1.95)	1.97 (1.97)	1.98 (1.96)	1.97	1.97
Fe(2)−N(12)	1.96 (1.96)	1.96 (1.97)	1.97 (1.97)	1.97 (1.94)	2.08	2.08
Fe(2)−N(13)	1.98 (1.97)	1.97 (1.96)	2.02 (2.01)	2.02 (1.98)	2.01	2.01
Fe(2)−N(14)	1.96 (1.96)	1.96 (1.95)	1.97 (1.97)	1.97 (1.98)	1.97	2.10
Fe(2)−N(15)	1.94 (1.95)	1.96 (1.94)	1.95 (1.98)	1.95 (1.95)	1.94	1.94
Fe(2)−N(16)	1.94 (1.93)	1.95 (1.93)	1.93 (1.94)	1.93 (1.93)	1.94	1.95
Fe(3)−N(17)	2.02 (1.98)	2.03 (1.99)	2.02 (2.01)	2.03 (2.00)	2.03	2.03
Fe(3)−N(18)	1.97 (1.97)	1.97 (1.96)	1.97 (1.97)	1.97 (1.96)	1.97	1.98
Fe(3)−N(19)	2.02 (1.96)	2.02 (1.98)	2.02 (1.97)	2.03 (2.00)	2.03	2.03
Fe(3)−N(20)	1.97 (1.95)	1.97 (1.96)	1.97 (1.97)	1.97 (1.92)	1.97	1.97
Fe(3)−C(21)	1.89 (1.91)	1.89 (1.89)	1.89 (1.90)	1.90 (1.92)	1.90	1.90
Fe(3)−C(22)	1.89 (1.93)	1.90 (1.88)	1.89 (1.93)	1.89 (1.90)	1.89	1.89
Fe(4)−N(23)	1.98 (1.96)	1.97 (1.95)	2.02 (2.00)	1.98 (1.96)	1.97	1.97
Fe(4)−N(24)	1.96 (1.97)	1.96 (1.95)	1.98 (1.98)	1.97 (1.94)	2.08	2.08
Fe(4)−N(25)	1.98 (1.98)	1.97 (1.96)	1.97 (1.97)	2.02 (1.98)	2.01	2.01
Fe(4)−N(26)	1.96 (1.96)	1.96 (1.97)	1.97 (1.97)	1.97 (1.98)	1.97	2.09
Fe(4)−N(27)	1.94 (1.94)	1.95 (1.94)	1.93 (1.93)	1.95 (1.95)	1.94	1.94
Fe(4)−N(28)	1.94 (1.93)	1.94 (1.93)	1.95 (1.94)	1.93 (1.93)	1.94	1.95

[a] Available X-ray structural data are given in parentheses. [b] The X-ray structural data collected at 293 K (ref 34). [c] The X-ray structural data collected at 200 K (ref 38). [d] The X-ray structural data collected at 100 K (ref 36). [e] The X-ray structural data collected at 100 K (ref 37).

collected in Tables 1−3. For comparison, the available X-ray crystallographic data are given in parentheses. For the [HS−HS] state, where the exchange coupling can generate a series of spin multiplets with the total spin value varying from 0 to 4, we considered the state with the highest total spin (the only state represented by a single-determinant wave function), supposing that the structure is not very sensitive to the total spin value when local spins are fixed. The atom numbering used throughout the paper is shown in Figure 1. From Tables 1−3 it can be seen that the optimized structural parameters are in a good agreement with the reported crystal data. As it usually is in DFT calculations, the agreement is better for the LS coordination cores.

The close inspection of the optimized geometries reveals a few interesting features. In the optimized structures, the $\{Fe_4(\mu\text{-}CN)_4\}$ core possesses a planar geometry in the case of **1** only. In all other complexes, the coordinated polydentate ligands induce a distortion of the $\{Fe_4(\mu\text{-}CN)_4\}$ core from planarity. In **2**, the terminal ligands around the Fe(3) and Fe(4) centers are coordinated in a different manner compared to the corresponding ligands in **1** (see Figure 1). As a result, the bpy and bpym ligands at neighboring iron centers form a network of relatively short intramolecular contacts. Thus, **2** is sterically more strained, and its optimized structures display a distorted square fragment (for any one of the three spin states). In **3**, the Fe(1) and Fe(3) centers are similar to those in **2** (see Figure 1); the coordination spheres of the Fe(2) and Fe(4) centers are completed by the tpma ligands. Compared to **3**, the tpma ligand around the Fe(4) center in **4** is coordinated in a different manner. As a result, the Fe(2)−N_{amine} and Fe(4)−N_{amine} bonds are directed along the mutually orthogonal axes in **3**, whereas these bonds are collinear in **4** (see Figure 1). It can be also seen that the phen ligands around the Fe(1) and Fe(3) centers in **4** are coordinated in the same manner as the bpy ligands in **1**. The $\{Fe_4(\mu\text{-}CN)_4\}$ core is slightly distorted in the **3** optimized structures, whereas it adopts a bent conformation in the **4** optimized structures.

Table 2. Selected Bond Lengths (Å) in Optimized (PBE/3z) and Experimental Structures of **1**−**6** in the [HS−LS] State[a]

	1	2	3	4	5	6
Fe(1)−N(5)	2.02	2.02	2.02 (1.98)[b]	2.03	2.03	2.03
Fe(1)−N(6)	1.97	1.97	1.97 (1.96)	1.98	1.98	1.98
Fe(1)−N(7)	2.02	2.03	2.03 (2.00)	2.04	2.04	2.04
Fe(1)−N(8)	1.97	1.97	1.97 (1.98)	1.97	1.97	1.97
Fe(1)−C(9)	1.87	1.87	1.87 (1.88)	1.86	1.86	1.86
Fe(1)−C(10)	1.90	1.89	1.91 (1.92)	1.89	1.90	1.89
Fe(2)−N(11)	2.25	2.27	2.25 (2.21)	2.25	2.22	2.20
Fe(2)−N(12)	2.18	2.18	2.22 (2.17)	2.21	2.32	2.39
Fe(2)−N(13)	2.25	2.28	2.33 (2.23)	2.33	2.31	2.28
Fe(2)−N(14)	2.18	2.18	2.21 (2.18)	2.21	2.22	2.36
Fe(2)−N(15)	2.08	2.08	2.10 (2.11)	2.10	2.09	2.08
Fe(2)−N(16)	2.08	2.07	2.06 (2.04)	2.05	2.07	2.06
Fe(3)−N(17)	2.02	2.03	2.03 (2.01)	2.04	2.04	2.04
Fe(3)−N(18)	1.97	1.97	1.97 (1.96)	1.97	1.97	1.98
Fe(3)−N(19)	2.02	2.02	2.02 (1.98)	2.03	2.03	2.03
Fe(3)−N(20)	1.97	1.97	1.97 (1.98)	1.97	1.98	1.98
Fe(3)−C(21)	1.90	1.89	1.90 (1.89)	1.90	1.90	1.90
Fe(3)−C(22)	1.87	1.87	1.88 (1.92)	1.87	1.87	1.87
Fe(4)−N(23)	1.98	1.97	2.02 (2.00)	1.98	1.97	1.97
Fe(4)−N(24)	1.96	1.96	1.98 (1.98)	1.98	2.08	2.08
Fe(4)−N(25)	1.98	1.97	1.98 (1.97)	2.02	2.01	2.01
Fe(4)−N(26)	1.96	1.96	1.98 (1.97)	1.97	1.97	2.10
Fe(4)−N(27)	1.94	1.95	1.93 (1.93)	1.95	1.95	1.95
Fe(4)−N(28)	1.94	1.94	1.95 (1.94)	1.93	1.94	1.95

[a] Available X-ray structural data are given in parentheses. [b] The X-ray structural data collected at 200 K (ref 36).

Complexes **5** and **6** are similar to **4** (see Figure 1), and their optimized structures display the same features.

Another aspect should be highlighted when discussing the data in Tables 1−3. In the optimized structures, the structural *trans* effect[61] of the CN ligand is clearly observed: the Fe−N bonds *trans* to the carbon or nitrogen atoms of the cyanide bridges are longer than those *cis* to the CN ligands. With a few exceptions, this is the case for all complexes in all three spin states. In **5** and **6**, the tpma ligand contains the methyl

(61) Coe, B. J.; Glenwright, S. J. *Coord. Chem. Rev.* **2000**, *203*, 5.

Table 3. Selected Bond Lengths (Å) in Optimized (PBE/3z) and Experimental Structures of **1**−**6** in the [HS−HS] State[a]

	1	2	3	4	5	6
Fe(1)−N(5)	2.02	2.03	2.03	2.04 (2.05)[b]	2.04 (2.00)[c]	2.04 (2.02)[d]
Fe(1)−N(6)	1.97	1.97	1.97	1.98 (1.98)	1.98 (1.97)	1.98 (1.97)
Fe(1)−N(7)	2.02	2.03	2.03	2.04 (2.02)	2.04 (1.99)	2.04 (1.99)
Fe(1)−N(8)	1.97	1.97	1.97	1.98 (1.93)	1.98 (1.97)	1.98 (1.95)
Fe(1)−C(9)	1.87	1.87	1.87	1.86 (1.91)	1.87 (1.92)	1.87 (1.90)
Fe(1)−C(10)	1.87	1.88	1.87	1.88 (1.92)	1.88 (1.91)	1.88 (1.92)
Fe(2)−N(11)	2.25	2.27	2.26	2.25 (2.18)	2.24 (2.21)	2.21 (2.20)
Fe(2)−N(12)	2.18	2.19	2.22	2.21 (2.18)	2.31 (2.26)	2.40 (2.35)
Fe(2)−N(13)	2.26	2.27	2.32	2.33 (2.18)	2.32 (2.24)	2.29 (2.22)
Fe(2)−N(14)	2.18	2.18	2.20	2.20 (2.20)	2.23 (2.22)	2.36 (2.29)
Fe(2)−N(15)	2.08	2.09	2.09	2.11 (2.07)	2.10 (2.08)	2.09 (2.09)
Fe(2)−N(16)	2.08	2.07	2.06	2.04 (2.02)	2.07 (2.04)	2.06 (2.08)
Fe(3)−N(17)	2.02	2.03	2.02	2.04 (2.05)	2.04 (2.00)	2.04 (2.02)
Fe(3)−N(18)	1.97	1.97	1.97	1.98 (1.98)	1.98 (1.97)	1.98 (1.97)
Fe(3)−N(19)	2.02	2.03	2.02	2.04 (2.02)	2.04 (1.99)	2.04 (1.99)
Fe(3)−N(20)	1.97	1.97	1.97	1.98 (1.93)	1.98 (1.97)	1.98 (1.95)
Fe(3)−C(21)	1.87	1.87	1.88	1.86 (1.91)	1.87 (1.92)	1.86 (1.90)
Fe(3)−C(22)	1.87	1.88	1.88	1.88 (1.92)	1.88 (1.91)	1.87 (1.92)
Fe(4)−N(23)	2.26	2.28	2.32	2.25 (2.18)	2.23 (2.21)	2.21 (2.20)
Fe(4)−N(24)	2.18	2.17	2.20	2.21 (2.18)	2.31 (2.26)	2.39 (2.35)
Fe(4)−N(25)	2.25	2.27	2.26	2.33 (2.18)	2.32 (2.24)	2.28 (2.22)
Fe(4)−N(26)	2.18	2.19	2.22	2.20 (2.20)	2.23 (2.22)	2.36 (2.29)
Fe(4)−N(27)	2.08	2.08	2.06	2.11 (2.07)	2.10 (2.08)	2.09 (2.09)
Fe(4)−N(28)	2.08	2.07	2.09	2.04 (2.02)	2.07 (2.04)	2.06 (2.08)

[a] Available X-ray structural data are given in parentheses. [b] The X-ray structural data collected at 370 K (ref 37). [c] The X-ray structural data collected at 293 K (ref 37). [d] The X-ray structural data collected at 160 K (ref 37).

substituent in the sixth position (adjacent to the donor atom) of one (**5**) or two (**6**) pyrid-2-ylmethyl moieties. The imine nitrogen atoms from the Me-substituted rings are in the *cis* positions to the nitrogen atoms of the cyanide bridges, but the corresponding Fe−N_{imine} bonds are strongly elongated due to the steric effects.[62] It can be seen that for all complexes the Fe−N bonds *trans* to the CN ligands are elongated to a larger extent in the course of the LS → HS transition. As a result, a stretching of the bonds due to the structural *trans* effect is best seen for the HS state. The amine nitrogen atom of the tpma ligand at a given transiting center (**3**−**6**) is in the *trans* position to the nitrogen atom of the cyanide bridge. It is worthy of note that the corresponding Fe−N_{amine} bond is longer than the adjacent Fe−N_{imine} bond *trans* to the CN ligand. This observation is again best seen for the HS state. Although DFT methods have a tendency to overestimate the Fe−L bond lengths, the calculated values reflect the structural features of the isolated molecules. These features are retained in the available crystal structures; however, they can be quenched by the crystal packing effects. For example, in the [HS−HS] isomer of **4**, the {$Fe_4(\mu$-CN)$_4$} core is in a bent conformation in the optimized structure, whereas in the crystal lattice it is flattened to some extent and adopts a distorted square geometry. As a result, the experimental Fe−N_L bond lengths for the transiting centers do not match the optimized ones.

To detect the factors giving rise to different types of SCO behavior, we performed a comparative analysis of the optimized FeN_6 geometries for all complexes of the series. At the first stage, it is important to analyze the changes in the coordination polyhedron of a given transiting center within the [LS−LS] and the [HS−HS] subsets of structures. In the optimized structures, the two transiting centers, Fe(2) and Fe(4), have very similar FeN_6 geometries; the Fe−N distances are given in Tables 1 and 3. In the [LS−LS] state (see Table 1), these distances are similar for **1** and **2**. An increase in one of the Fe−N distances is observed in **3** (Fe−N_{amine} = 2.02 Å). In **4**, the distances are similar to those in **3**. In **5**, one more Fe−N distance increases, namely the distance to the nitrogen atom from the Me-substituted ring of the tpma ligand (2.08 Å). In **6**, the tpma ligand contains one more Me-substituted ring, and therefore the corresponding Fe−N distance is also increased (2.10 Å). Even more pronounced increase in the Fe−N bond lengths is observed for the [HS−HS] state (see Table 3). Thus, one may say about a weakening of the ligand field at the transiting centers in the given series of compounds.

Another important question concerns the ligand strain effects, which might stabilize the mixed [HS−LS] state. These effects are inherent to the isolated molecules, and therefore the analysis of the optimized structures of the three spin-state isomers allows to conclude whether the steric strain effects reveal themselves in a given species. The role of these effects was highlighted in ref 28. It was demonstrated that, in the case of sterically strained binuclear complexes, the SCO on one site may cause a distortion of the geometry around the other site. Therefore, in the present work, for each complex we analyzed the geometry around the first transiting center, Fe(2), in the [HS−HS] and [HS−LS] states. However, we did not find any changes, which might weaken the ligand field and stabilize the HS state at this site in the [HS−LS] state. For similar reasons, we analyzed the geometry around the second transiting center, Fe(4), in the [LS−LS] and [HS−LS] states, but no changes, which might strengthen the ligand field and stabilize the LS state at this site in the [HS−LS] state, were found. Thus, in the optimized structures, we did not reveal any distortions, which might stabilize the intermediate spin state.

The relative energies of the three spin states calculated at the optimized geometries are given in Table 4a. For all complexes, the [LS−LS] state was found to be the ground state, and its energy was taken as zero. Our calculations predict a decrease in the energy gaps between the spin states, which is consistent with the conclusion about a weakening of the ligand field at the transiting centers in the given series of compounds (see the above discussion). According to calculations, the [HS−LS] and [HS−HS] states are strongly destabilized in **1** and **2** containing the strong field ligands (bpy and bpym, respectively) at the transiting centers. These states, however, are slightly stabilized in **2** compared to **1**. The presence of the remote nitrogen atoms in the bpym ligand causes a decrease in the σ-donor character (weakens the metal−ligand interaction) and an increase in the π-acceptor character (strengthens the metal−ligand interaction). An increase in the optimized Fe−L bond lengths in **2** observed for the HS FeN_6 coordination cores suggests that the net effect of the modification of the diimine ligand is a slight weakening of the metal−ligand interaction (i.e., the bpym ligand produces a slightly weaker field). A slight stabilization of the [HS−LS] and [HS−HS] states in **2** compared to **1** also reflects this fact. It should be noted that complexes **1** and **2** differ not only in their chemical composition but also in their stereochemistry. The absolute configuration of iron centers in **1** is ΔΔΔΔ, whereas in **2** it is ΔΔΛΔ. However, this difference in the helicity of nontransiting iron centers does not provide an important perturbation to modify the spin-state energetics imposed by electronically close diimine ligands. The tpma ligands in **3** and **4** stabilize the [HS−LS]

(62) Goodwin, H. A. *Top. Curr. Chem.* **2004**, *233*, 59.

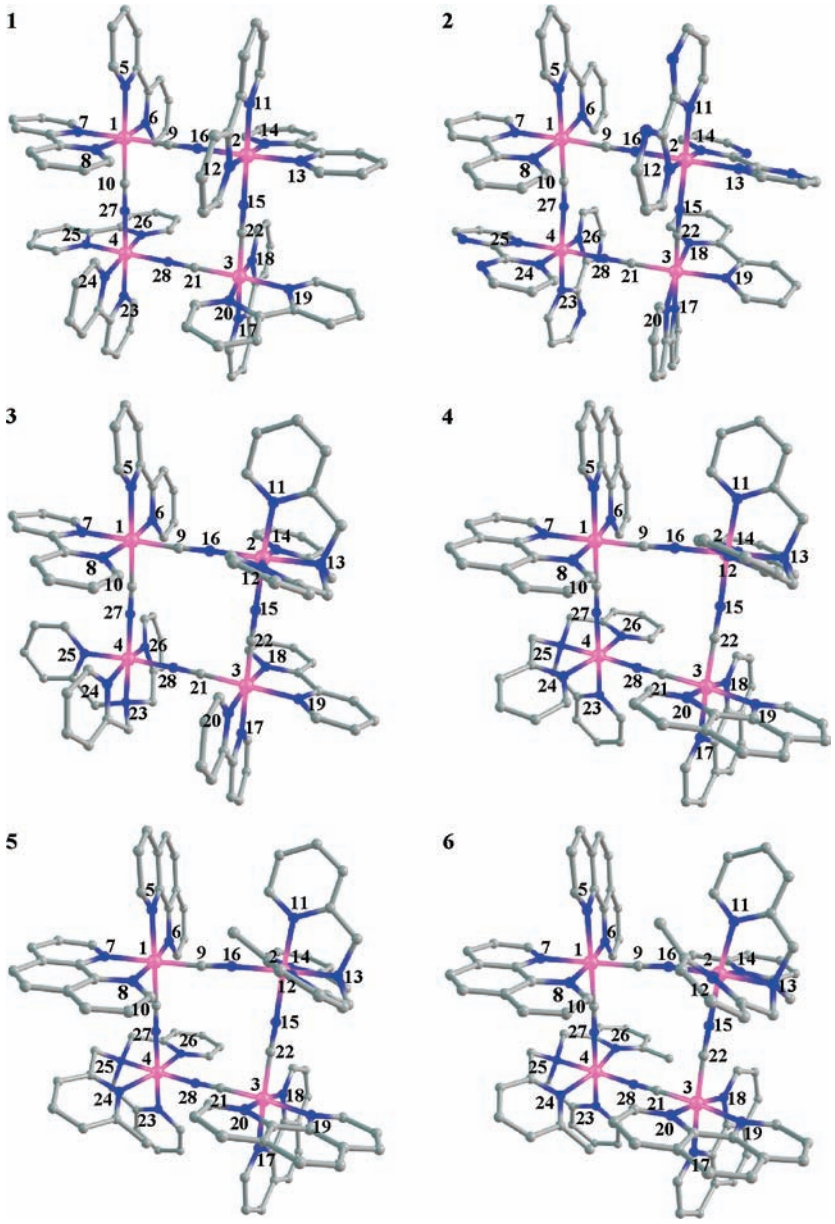

Figure 1. Molecular structures of **1**−**6** (optimized structures in the [LS−LS] state are presented; hydrogen atoms are not included for the sake of simplicity).

and [HS−HS] states to a much larger extent. In **5** and **6** containing Me-substituted tpma ligands, the methyl substituents generate the steric hindrance in the FeN_6 coordination cores, and so, these states are strongly stabilized. The results of calculations are in a qualitative agreement with the magnetic susceptibility data (reported in refs 34 and 36−38 and mentioned in the Introduction), with the exception of complexes **5** and **6**, for which calculations do not reproduce the ground state inversion.

Complexes **3** and **4** deserve a more thorough consideration. In these species, the tpma ligands produce the field of approximately equal strength; however, the transiting centers in **4** change the spin state simultaneously, whereas in **3** one of them undergoes the spin transition at lower temperature. It was mentioned in the Introduction that, when the mixed [HS−LS] state falls in the energy gap between the [LS−LS] and [HS−HS] states, the shaping of the spin transition is determined by the relative position of the intermediate spin state. According to the conclusion of the thermodynamical model,[20] the enthalpy of the [HS−LS] state must be lower than the average enthalpy of the [LS−LS] and [HS−HS] states to have a two-step SCO. Our analysis of the optimized structures does not reveal any structural changes, which might favor energetically the mixed spin state (see the above discussion). Indeed, from Table 4a it can be seen that the [HS−LS] state for all complexes lies about in the middle of the energy gap between the [LS−LS] and [HS−HS] ($S = 4$) states. It follows that, in the isolated complexes, the transiting centers are independent (elastic interactions between them are weak) and should change the spin state independently. However, as we mentioned before, one SCO center in **3** undergoes the spin transition at lower temperature. This deviation from the isolated molecule behavior should be attributed to the crystal lattice effects.

Before discussing the role of crystal packing effects, we would like to stress again that the donor atoms of the

Table 4. Relative Energies of the [LS−LS], [HS−LS], and [HS−HS] States for **1**−**6** (in kJ mol^{-1})

(a) relative energies of the structurally optimized [LS−LS], [HS−LS], and [HS−HS] states

	[LS−LS]	[HS−LS]	[HS−HS]
1	0.0	93.8	186.8
2	0.0	92.0	186.1
3	0.0	74.1	147.5
4	0.0	75.0	147.3
5	0.0	58.0	109.9
6	0.0	34.8	67.0

(b) "vertical" energies of different spin states at the geometries optimized for the [LS−LS] and [HS−LS] states

	[LS−LS] geometry			[HS−LS] geometry	
	[LS−LS]	[HS−LS]	[HS−HS]	[HS−LS]	[HS−HS]
1	0.0	232.8	465.7	93.8	325.7
2	0.0	241.4	485.7	92.0	336.5
3	0.0	212.7	424.9	74.1	285.3
4	0.0	212.8	425.9	75.0	286.0
5	0.0	191.1	381.9	58.0	246.2
6	0.0	159.1	318.6	34.8	191.0

polydentate ligands in **3** and **4** complete the coordination spheres of iron centers in a different manner (see the above discussion and Figure 1). The differences in coordination of the terminal ligands predetermine the crystal packing motif of the corresponding compounds, **3**$(PF_6)_4$ and **4**$(PF_6)_4$. The latter crystallizes in the monoclinic $C2/c$ space group and displays the structurally equivalent diagonal iron sites, which is consistent with a simultaneous SCO on both transiting centers. The former displays the triclinic $P\bar{1}$ space group, and in this case the $\{Fe_4(\mu\text{-}CN)_4\}$ core does not have any elements of symmetry. In the three available crystal structures of **3**$(PF_6)_4$ corresponding to the [LS−LS] (100 K) and [HS−LS] (200 and 300 K) phases,[36] the tpma ligands around the Fe(2) centers possessed by two neighboring tetranuclear species are involved in a strong $\pi-\pi$ interaction, which causes a noticeable deviation of one of the two Fe(2)−N−C bond angles from 180°. Such distortion results in an increase in the corresponding Fe(2)−N bond length. These distortions are lacking in the optimized structures of **3**. In contrast, there are no short intermolecular contacts between the rings of the tpma ligands around the Fe(4) centers, and the geometry around the Fe(4) center (similar in all three crystal structures) is similar to that in the optimized [LS−LS] and [HS−LS] structures of **3**. It is evident that, due to the distortions induced by the intermolecular interactions in the crystal, the Fe(2) site is in a weaker ligand field compared to the Fe(4) site. The crystal structures of **4**$(PF_6)_4$ corresponding to the [LS−LS] (100 K) and [HS−HS] (370 K) phases[37] are free of these distortions. Thus, it is precisely the intermolecular interactions that are responsible for the stabilization of the [HS−LS] state in **3**$(PF_6)_4$. It is important also to note that the geometry around the LS transiting centers in **4**$(PF_6)_4$ is similar to the geometry around the Fe(4) center in **3**$(PF_6)_4$, i.e., the ligand field at these centers is of approximately equal strength. The corresponding [Fe(tpma)$(NC)_2$] fragments in **3**$(PF_6)_4$ and **4**$(PF_6)_4$ have more or less equivalent networks of intermolecular contacts. Indeed, the SCO on these sites takes place in the same temperature interval.

Table 5. Octahedricity and Trigonal Prismacity Values for the Fe(2) and Fe(4) Centers in Crystal Structures of **3** (100, 200, and 300 K) and Optimized Structures for Three Spin States

	octahedricity[a]		trigonal prismacity[a]	
	Fe(2)	Fe(4)	Fe(2)	Fe(4)
100 K	0.58	0.31	13.39	14.41
[LS−LS]	(0.31)	(0.31)	(15.06)	(15.06)
200 K	1.80	0.30	11.33	14.35
[HS−LS]	(1.29)	(0.30)	(13.71)	(14.98)
300 K	1.83	0.33	11.33	14.43
[HS−HS]	(1.30)	(1.30)	(13.35)	(13.35)

[a] These parameters have zero values for ideal octahedron and trigonal prism.

Finally, we would like to discuss the CShM data characterizing the shape of coordination polyhedra of transiting centers in the crystal structures of **3** as well as in the optimized structures for the three spin states. The octahedricity and trigonal prismacity values are given in Table 5. It can be seen that at any temperature these values for the Fe(4) center are close to those for the LS center in the isolated complex. The situation is somewhat different for the Fe(2) center. At 300 K its octahedricity and trigonal prismacity are respectively higher and lower than those for the HS state in the isolated complex. This deviation can be explained only by the influence of crystal environment. At 200 K the Fe(2) polyhedron slightly approaches the LS characteristics, but only its 100 K parameters display a well-developed HS → LS transformation. However, again the values deviate from the corresponding values for the isolated complex. The comparison of the CShM values for the optimized structures, for which the Fe(2) and Fe(4) centers have been supposed symmetrically equivalent in the [LS−LS] and [HS−HS] states, and the experimental geometries with the nonequivalent Fe(2) and Fe(4) centers allows to conclude that the SCO on the Fe(4) center occurs as in the isolated cation, whereas for the Fe(2) center it is strongly influenced by crystal packing effects. This conclusion is in line with all our previous findings, linking the two-step SCO in **3** with intermolecular effects. Unfortunately, the lack of variable temperature X-ray data does not allow to extend such analysis on other complexes.

In the above discussion, on the basis of relative energies of the structurally optimized [LS−LS], [HS−LS], and [HS−HS] ($S = 4$) states (Table 4a), we drew an important conclusion, which refers equally to all complexes of the series. The mixed spin state for all complexes lies about in the middle of the energy gap between the homogeneous spin states, thereby satisfying the conditions for an one-step SCO between the [LS−LS] and [HS−HS]. Thus, we concluded that, in the isolated complexes, the transiting centers are independent (elastic interactions between them are weak). Interestingly, the structural data collected in Tables 1−3 lend an additional support to this conclusion. Thus, for all complexes the expansion of the FeN_6 coordination sphere of the first transiting center, Fe(2), on going from LS to HS state causes some contraction (up to 0.04 Å) of the bonds between the neighboring iron centers and the carbon atoms of the CN ligands bridging to Fe(2). A slight lengthening of the two other Fe(1)/Fe(3)−C bonds is also observed, whereas the bond lengths around the second transiting center, Fe(4), stay invariant. Similarly, the contraction of the Fe(4)−N bonds on going from HS to LS state causes some lengthening (up to 0.04 Å) of the bonds between the non-SCO centers and the

carbon atoms of the CN ligands bridging to Fe(4). A slight contraction of the two other Fe(1)/Fe(3)−C bonds is also observed, whereas the bond lengths around Fe(2) stay invariant (see also the above discussion on the ligand strain effects). Thus, the distortion caused by the SCO on one center seems to be fully absorbed by the FeN_4C_2 sites and is not transferred to another SCO center.

Along with the energies at the equilibrium spin-state geometries, we calculated the energies of different spin states at the geometries optimized for one of them (Table 4b). It can be seen that for all complexes the energies of the vertical transition from the [LS−LS] to the [HS−LS] state is about the same as from the [HS−LS] to the [HS−HS] ($S = 4$) state. This fact again reflects the weak elastic coupling between the transiting centers. In other words, according to our results, the change of the spin state at one center does not affect the transition energy of another center. In terms of the SCO cooperativity, one can say that cyanide-bridged iron(II) squares are characterized by a very weak intramolecular cooperativity.

The important effect, which might change the above conclusion, is the exchange coupling between the paramagnetic ions in the [HS−HS] state. The exchange interactions (if effective) split the [HS−HS] state into spin multiplets. The cyanide ion is well-known as an efficient transmitter of magnetic interactions between paramagnetic ions.[63] In complexes **1**−**6**, the two transiting centers are well separated by the diamagnetic $[Fe(L)_2(CN)_2]$ fragments (L = bpy or phen), and therefore the exchange coupling in the [HS−HS] spin-state isomers should be weak. Indeed, the J values computed for the optimized [HS−HS] geometries and available crystal structures are rather small and correspond to ferromagnetic coupling (Table S4 of the Supporting Information). For example, for **3** and **4**, either of the three schemes (eqs 1−3) gives the J value equal to 0.3 and 0.3 (0.2) cm^{-1}, respectively. The value in parentheses corresponds to the [HS−HS] crystal structure available for **4**. In such a case, the five exchange multiplets relating to the [HS−HS] state are nearly degenerate, and the splitting (the energy interval between the ground $S = 4$ and highly excited $S = 0$ levels is equal to $10J$) does not influence the total energetics of SCO. We would like also to note that the computed J values agree with the weak ferromagnetic interactions through the NC−M−CN bridges observed in the Prussian blue analogues.[64]

Conclusions

Our calculations for a series of cyanide-bridged iron(II) square complexes allow to formulate several conclusions.

The elastic coupling between the transiting iron(II) centers in these complexes is rather weak and does not satisfy the conditions necessary for the stabilization of the intermediate [HS−LS] state. The multistability of these quasi-binuclear systems can result only from the crystal packing effects. In $\mathbf{3}(PF_6)_4$, the $[Fe(2)(tpma)(NC)_2]$ and $[Fe(4)(tpma)(NC)_2]$ fragments have different networks of intermolecular contacts, and it is precisely the intermolecular interactions that are responsible for the stabilization of the [HS−LS] state.

The short-range elastic interactions through the CN bridges are weak and do not provide an efficient mechanism for the SCO cooperativity. It differs molecular CN-bridged systems from solid Prussian blue analogues, where the long-range interactions can lead to a cooperative SCO, even with a hysteresis.[64,65]

These conclusions can be changed for other iron(II) square complexes with more complex bridging ligands. Work is in progress to characterize structural and electronic aspects of the SCO in other known iron(II) squares.

Acknowledgment. The authors thank Dr. Galina S. Matouzenko for useful discussions and valuable help. We also thank the referees for their useful comments.

Supporting Information Available: Three tables containing the results of test calculations, one table showing the J values for the [HS−HS] state computed for optimized and available crystal structures of the complexes. This material is available free of charge via the Internet at http://pubs.acs.org.

(63) Verdaguer, M.; Bleuzen, A.; Marvaud, V.; Vaissermann, J.; Seuleiman, M.; Desplanches, C.; Scuiller, A.; Train, C.; Garde, R.; Gelly, G.; Lomenech, C.; Rosenman, I.; Veillet, P.; Cartier, C.; Villain, F. *Coord. Chem. Rev.* **1999**, *190*−*192*, 1023.

(64) Kosaka, W.; Nomura, K.; Hashimoto, K.; Ohkoshi, S. *J. Am. Chem. Soc.* **2005**, *127*, 8590.

(65) Le Guennic, B.; Borshch, S. A.; Robert, V. *Inorg. Chem.* **2007**, *46*, 11106.